Elastic indentation of a rough surface by a conical punch

Noname manuscript No.
(will be inserted by the editor)

Elastic indentation of a rough surface by a conical punch

Mauro Borri-Brunetto · Michele Ciavarella

the date of receipt and acceptance should be inserted later

Abstract In the contact of a cone with a rough plane the mean pressure in the contact area is constant. In particular, above a critical ratio of the opening angle of the cone with respect to the rms gradient of surface roughness, the mean pressure is the same of that for nominally flat contact, no matter how large is the normal load. We introduce a new variable, namely, the local density of contact area, whose integral over the smooth nominal contact domain gives the real contact area. The results given by the theoretical model agree with the numerical simulations of the same problem presented in the paper.

Keywords Contact mechanics · Contact area · Numerical analysis · Analytical model

1 Introduction

Indentation techniques are useful to measure the elastic properties of solids from large to very small volumes, the latter case being particularly useful for thin coatings, or in general heterogeneous materials (see e.g.the review by Gibson [1]). The classical solution for frictionless conical indentation was found by Love [2] and it has been largely used [e.g., 3, 4]. Nevertheless, to the best of the authors' knowledge, the question of the influence of roughness on the conical tip indentation has not been discussed.

M. Borri-Brunetto
Department of Structural, Geotechnical and Building Engineering, Politecnico di Torino, Corso Duca degli Abruzzi 24, 10129 Torino, Italy, E-mail: mauro.borri@polito.it

M. Ciavarella
Department of Mechanics, Mathematics and Management, Politecnico di Bari, Viale Japigia 182, 70125 Bari, Italy E-mail: michele.ciavarella@poliba.it

Recently, Pastewka and Robbins [5] have shown that in the contact of a sphere with a rough plane there are three regimes of behaviour. Namely, for increasing applied normal loads the contact starts off in a regime dominated by a single asperity, then there is a regime of linearity between real contact area and load, where there is no influence of the curvature of the sphere (and hence the mean pressure is the same as in the contact of nominally flat surfaces), and finally there is a crossover towards the contact of the sphere on a smooth plane.

The case of a nominally flat rough contact has been studied in depth and Persson has devised an ingenious diffusion process solution [6], which gives an approximate expression of the real contact area ratio (A_0 being the nominal contact area) as a function of mean pressure p_m, which is linear at low pressures. We will not use his solution, but an improved one:

$$\frac{A}{A_0} = \mathrm{erf}\left(\frac{\sqrt{\pi}}{2}\frac{p_m}{p_{\mathrm{rough}}}\right) \approx \frac{p_m}{p_{\mathrm{rough}}} + O\left[\left(\frac{p_m}{p_{\mathrm{rough}}}\right)^3\right]. \quad (1)$$

In the following, we use the full solution given by the left relation of eq. (1), particularly because the nominal contact pressure tends to very high values for a cone, with a singularity at the apex. This is an expression similar to that of Persson's theory (see Appendix), where a characteristic pressure is defined as

$$p_{\mathrm{rough}} = h'_{\mathrm{rms}} E^*/k \quad (2)$$

and $k \approx 2$ according to numerical investigations [7, 8]. Here, E^* is the plane strain composite elastic modulus of the materials, and $h'_{\mathrm{rms}} = \sqrt{\langle|\nabla h|^2\rangle}$ is the root mean square of the areal roughness gradient. In eq. (1), missing the quadratic term, the linear term is dominant up to area ratios of the order of 50 % or so.

The growth of the contact area with applied pressurehas been demonstrated numerically [9, 10] to depend not only on $h'_{\rm rms}$ but also on other roughness characteristics, notably on Nayak's parameter. However, this was here considered not to be relevant for a first order solution.

In the very initial stages of the loading process a single asperity is in contact with the sphere, and the behaviour is ruled by the asperity equivalent radius. For increasing load, when a sufficient number of asperities are in contact, Pastewka and Robbins suggested a simplification of Persson's solution, using as mean pressure p_m that of a Hertzian contact, i.e., $p_{m,s} = N/A_{\rm Hertz}$:

$$\frac{A}{A_{\rm Hertz}} = \text{erf}\left(\frac{\sqrt{\pi}}{2}\frac{N/A_{\rm Hertz}}{p_{\rm rough}}\right), \tag{3}$$

where $A_{\rm Hertz} = \pi a^2 = \pi\left(\frac{3NR}{4E^*}\right)^{2/3}$ is the Hertz contact area under the load N, and therefore scales as $N^{2/3}$. Here, a is the contact area radius, R is the radius of the sphere. When $N/A_{\rm Hertz}$ is low, this equation simply predicts linearity between real contact area and load. The mean pressure in the rough contact increases with load and hence the contact area tends to saturate asymptotically as a pure Hertzian contact without roughness. The crossover from the rough contact into the smooth Hertzian regime is obtained introducing the load N_c at which $\frac{N_c/A_{\rm Hertz}}{p_{\rm rough}} = 1$, i.e., $N_c = \pi^3\left(\frac{3}{4}\right)^2 (h'_{\rm rms}/2)^3 E^* R^2$.

Pastewka and Robbins found a picture which is simpler than Greenwood and Tripp [11], who introduced a distribution of asperities treated as a non-linear layer on an elastic sphere ruled by two dimensionless parameters, where there is a more dominant role of the rms amplitude of roughness, although they inevitably neglected the possibility that roughness plays a significant effect of "smearing out"the contact area.

In the present note we consider the case of a conical punch indenting an elastic halfspace bounded by a rough surface, studying the influence of the governing parameters on the evolution of the contact interface by means of theoretical analyses and numerical simulations, and we propose a simple model similar to Pastewka and Robbins [5].

2 Contact of a cone with a rough surface

2.1 Theoretical model

The mean pressure $p_{m,c}$ exerted by a cone indenting a smooth plane [2, 12, 13] is constant, independent of the load N, as expected on similarity grounds:

$$p_{m,c} = E^* \cot\alpha/2 \tag{4}$$

and the contact area increases linearly with the load, depending on the cone semi-opening angle α and on the elastic modulus:

$$A_{\rm cone} = \frac{2N}{E^* \cot\alpha}. \tag{5}$$

Extending the suggestion of Pastewka and Robbins (our eq. (3)) to the case of the cone, we can write

$$\left(\frac{A}{A_{\rm cone}}\right)_{\rm PR} = \text{erf}\left(\frac{\sqrt{\pi}}{2}\frac{p_{m,c}}{p_{\rm rough}}\right) = \text{erf}\left(\frac{\sqrt{\pi}}{2}\rho_c\right), \tag{6}$$

where the pressure ratio for the cone, $\rho_c = p_{m,c}/p_{\rm rough}$, has been introduced. By using eqs. (2) and (4), with $k = 2$, we have

$$\rho_c = \frac{\cot\alpha}{h'_{\rm rms}}, \tag{7}$$

i.e., a constant independent of the load, determined only by the geometry of the rough surface and of the indenter, which assumes the role of a normalized mean pressure.

In particular, if the semi-opening angle α is large with respect to the roughness $h'_{\rm rms}$(incidentally, to satisfy the assumptions of linear elasticity, we need large cone opening angles), i.e., $\cot\alpha \ll h'_{\rm rms}$, then eq. (6) can be linearized, and for small ρ_c

$$A \approx \rho_c A_{\rm cone} = \frac{2N}{E^* h'_{\rm rms}}, \tag{8}$$

so that the contact area is proportional to the load, independent of the cone angle, and therefore $p_m = p_{\rm rough} \approx h'_{\rm rms} E^*/2$.

This is the case for a very large opening angle and significant roughness. Viceversa, when $\rho_c = \cot\alpha/h'_{\rm rms}$ increases, the real contact area continues to be proportional to the load, but the proportionality factor, and hence the mean pressure, depend also on the cone opening angle:

$$A = \text{erf}\left(\frac{\sqrt{\pi}}{2}\frac{\cot\alpha}{h'_{\rm rms}}\right)\frac{2N}{E^* \cot\alpha}. \tag{9}$$

If we view this from a different perspective, starting off with the smooth case, the mean pressure increases until it tends to the value of the nominally flat rough contact. The main difference with respect to the spherical case, is that there is no longer a further saturation towards a smooth-contact regime, i.e., in other words, the effect of roughness never disappears.

Moreover, we suggest a more refined analysis defining a *local density of contact*, γ, which varies with the local pressure value, while Pastewka and Robbins's approximation corresponds to assuming a constant pressure. The function $\gamma(\mathbf{x})$ is defined, at a given point $\mathbf{x}$

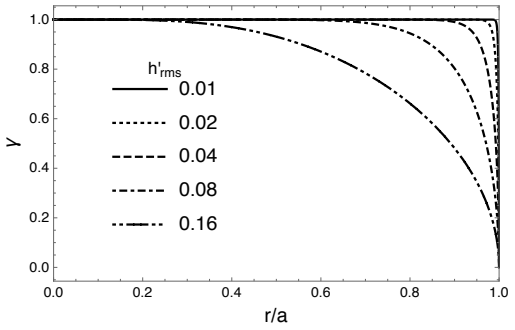

Fig. 1: Profile of the contact area density $\gamma(r)$ induced by a cone with semi-opening $\alpha = 80°$ against rough surfaces with different roughness $h'_{\rm rms}$. The corresponding values of ρ_c are given in Table 1

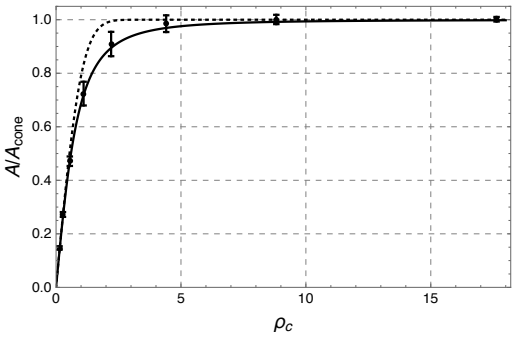

Fig. 2: Real contact area ratio vs. normalized mean pressure, ρ_c for a cone. Comparison of the numerical integration of the variable contact density (eq. (12), continuous curve) with the constant density approximation (eq. (6), dotted curve). Dots with error bars represent mean values and standard deviations obtained with numerical simulations (see sec. 2.2)

in the nominal contact domain, as the limit of the true contact area ratio for a disk of radius ϵ containing the point, for $\epsilon \to 0$.

In cases with radial symmetry it is a function of the radius r:

$$\gamma(r) = \operatorname{erf}\left(\frac{\sqrt{\pi}}{2}\frac{p(r)}{p_{\rm rough}}\right). \tag{10}$$

The normal pressure induced by a cone contacting a smooth halfspace on a disk of radius a [see, e.g., 14, p. 114] is

$$p(r) = p_{m,c}\cosh^{-1}\left(\frac{a}{r}\right), \quad 0 \le r \le a. \tag{11}$$

By inserting eq. (11) into eq.(10) one obtains the contact density as a function of the radius r. Figure 1 depicts the graphs of $\gamma(r)$ in the contact zone of a 80° cone, for different values of the roughness $h'_{\rm rms}$. As shown in the figure, the effect of increasing roughness is to deviate more and more from uniform contact density on the contact surface. It is interesting to note that the shape of the curves is unaffected by the total load N, which influences the contact domain only by increasing the contact radius a.

Given the expression of the density $\gamma(r)$ introduced above, the real contact area ratio can be evaluated as its integral over the circular contact domain:

$$\begin{aligned}\frac{A}{A_{\rm cone}} =& \frac{1}{\pi a^2}\int_0^a 2\pi r\gamma(r)\mathrm{d}r \\ =& \frac{2}{a^2}\int_0^a r\operatorname{erf}\left[\frac{\sqrt{\pi}}{2}\rho_c\cosh^{-1}\left(\frac{a}{r}\right)\right]\mathrm{d}r.\end{aligned} \tag{12}$$

It turns out that the integral in eq. (12) does not depend on the contact radius a and can be numerically integrated for any given value of ρ_c. Plotting the results as a function of ρ_c gives the continuous curve of Figure 2, where it is compared with the approximation corresponding to assuming uniform pressure (eq. (6)), similarly to what was done by Pastewka and Robbins for the sphere, represented by a dotted line. The difference between the two curves is larger in the intermediate range of ρ_c and vanishes for small and large values of the parameter.

2.2 Numerical simulations

The predictions of the rough-contact model described above have been compared to the results obtained with the numerical code *Icarus* [15, 16], applied to the simulation of contact between a conical indenter and a rough halfspace.

The code operates in an incremental-iterative way, considering the normal interaction of two contacting linear-elastic bodies through a grid of adjacent patches that discretize their surfaces. It permits to consider explicitly in the calculations the real topography of the rough surfaces at a given resolution and to evaluate the real contact area by counting the number n_p of patches where a local normal compressive force is exchanged between the bodies at an assigned approach. Rough surfaces can be generated, by means of several algorithms, with assigned roughness parameters as, in particular, the root mean square of the surface slopes, $h'_{\rm rms}$.

In general, recent approaches for roughness use self-affine fractal surfaces with power law PSD $A|\mathbf{q}|^{-2(1+H)}$ for wavevectors $q_r < |\mathbf{q}| < q_s$ ($q = 2\pi/\lambda$) with roll off to a constant for $q_0 < |\mathbf{q}| < q_r$ (generally limited to $x = q_0/q_r = 1/4$ or $1/2$) and zero otherwise. The general definition of the (even order) moments is reduced into the following form if the power spectrum density

(PSD), $C(q)$, is axisymmetric (e.g., the rough surface is isotropic):

$$\begin{aligned} m_n =& m_{n0} = \int_{q_0}^{q_s} \int_0^{2\pi} [q\cos(\theta)]^n \, C(q) q \, \mathrm{d}q \, \mathrm{d}\theta \\ =& T(n) \int_{q_0}^{q_s} C\left(q\right) q^{n+1} \mathrm{d}q \\ =& A\, T(n)\, q_r^{n-2H} \left(\frac{1-x^{n+2}}{n+2} + \frac{\zeta^{n-2H}-1}{n-2H} \right), \end{aligned} \quad (13)$$

where $T(n) = 2\pi, \pi, 3/4\pi$ $(n = 0, 2, 4)$, and we have introduced the "magnification" $\zeta = q_s/q_r \gg 1$, typically. Hence, knowing that $h_{\mathrm{rms}} = \sqrt{m_0}$, and $h'_{\mathrm{rms}} = \sqrt{2m_2}$, from the ratio of m_0 and m_2 we have, approximately:

$$\begin{aligned} \frac{h_{\mathrm{rms}}}{h'_{\mathrm{rms}}} \approx \frac{\sqrt{m_0}}{\sqrt{2m_2}} &= \frac{\sqrt{q_r^{-2H}\left(\frac{1-x^2}{2} + \frac{\zeta^{-2H}-1}{-2H}\right)}}{\sqrt{q_r^{2-2H}\left(\frac{1-x^4}{4} + \frac{\zeta^{2-2H}-1}{2-2H}\right)}} \\ &\approx \frac{\zeta^H}{q_s} \sqrt{\frac{\frac{1-x^2}{2} + \frac{1}{2H}}{\frac{1}{2-2H}}}. \end{aligned} \quad (14)$$

In our case, we do not use roll-off to the constant, but purely power-law (although this is known to introduce less gaussian heigths distribution), which means $x = 1$, and

$$h_{\mathrm{rms}} \approx h'_{\mathrm{rms}} \sqrt{\frac{1-H}{H}} \frac{\zeta^H}{q_s}, \quad (15)$$

which permits to estimate the rms amplitudes for given $h'_{\mathrm{rms}}, H, \zeta, q_s$.

In all the simulations presented here, the rough surfaces were generated on a grid of 512×512 square patches, each with side δ. This length represents the resolution of the simulation, i.e., the size of the smallest observable surface feature. The height of the patches were generated by means of a spectral synthesis algorithm [17], according to the roughness model of a self-affine surface with long distance rolloff and short distance cutoff wavelengths [18]. In order to obtain results comparable to the analytical findings reported in sec 2.1, we choose to generate families of surfaces with assigned h'_{rms} values. The Hurst exponent of the surfaces was 0.8, the small and large wavelength were 4δ and 512δ, respectively. The corresponding roughness h_{rms} can be estimated by using eq. (15).

We studied the contact of a single cone indenting the surface with an imposed approach such that the contact domain was completely included within the surface. Under this assumption there is no need of considering a periodic arrangement of multiple adjacent surface patches to enlarge the possible contact region.

The spectral properties of the generated surfaces were verified a posteriori according to the methods described by Jacobs et al [19]. Figure 3 shows an example of the typical distributions of slopes, heights and curvatures, and the power density spectrum of a generated surface.

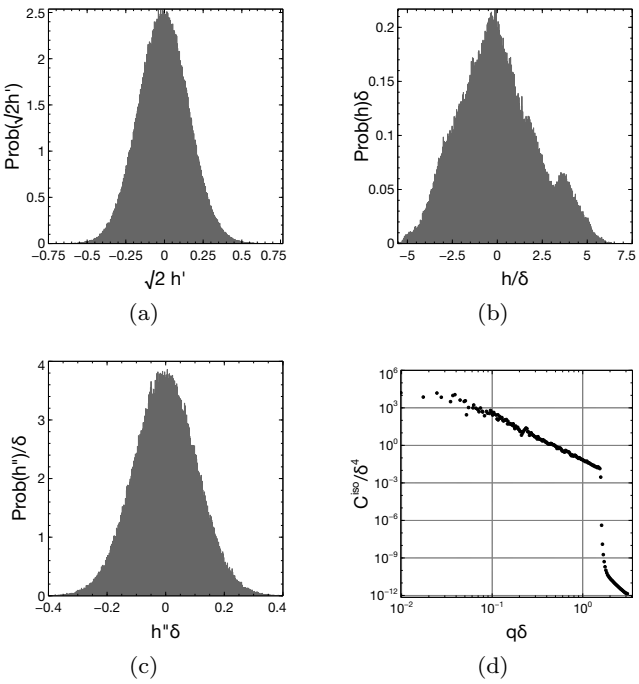

Fig. 3: Typical distribution of roughness quantities for a generated surface ($h'_{\mathrm{rms}} = 0.16$). (a) slope, (b) height, (c) curvature, and (d) power density spectrum. Two-dimensional power-spectral density $C^{\mathrm{iso}}(q)$ evaluated according to [19]. All values are normalized by using the grid spacing δ

For each value of the imposed displacement of the cone, the contact domain, i.e., the set of surface patches where compressive forces are exchanged between the contacting bodies, was determined. The total normal load N and the local forces at the contacting surface patches were calculated as well.

As an example, considering the case $\alpha = 80°$, Figure 4 shows the calculated contact domains, at approximately the same load N for the smooth case and five rough surfaces differing only in the h'_{rms} value. Each contact patch is coloured according to the value of the local compressive force.

The value of the real contact area ratio given by an Icarus simulation refers to a particular realization of the rough surface, which can be thought of as a random extraction from a population of surfaces with the same

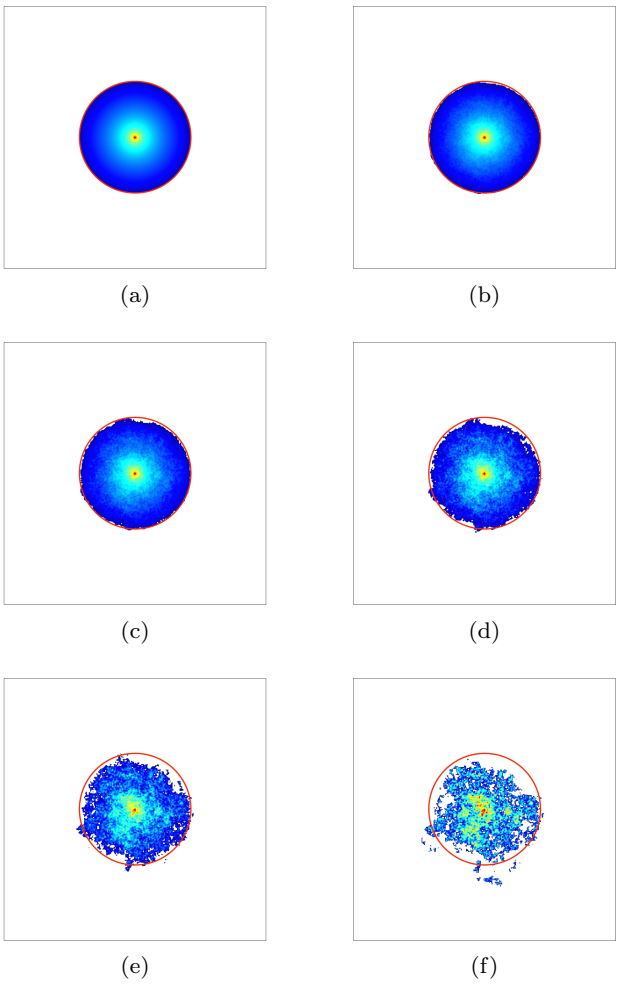

Fig. 4: Contact domains for a conical indenter with semi-opening $\alpha = 80°$, at the same load N and different increasing values of the halfspace roughness ((a) smooth surface; (b)-(f): $h'_{\rm rms} = 0.01, 0.02, 0.04, 0.08, 0.16$, respectively). The side of the boundary square corresponds to 512δ. The circle depicts the contact area of the smooth surface

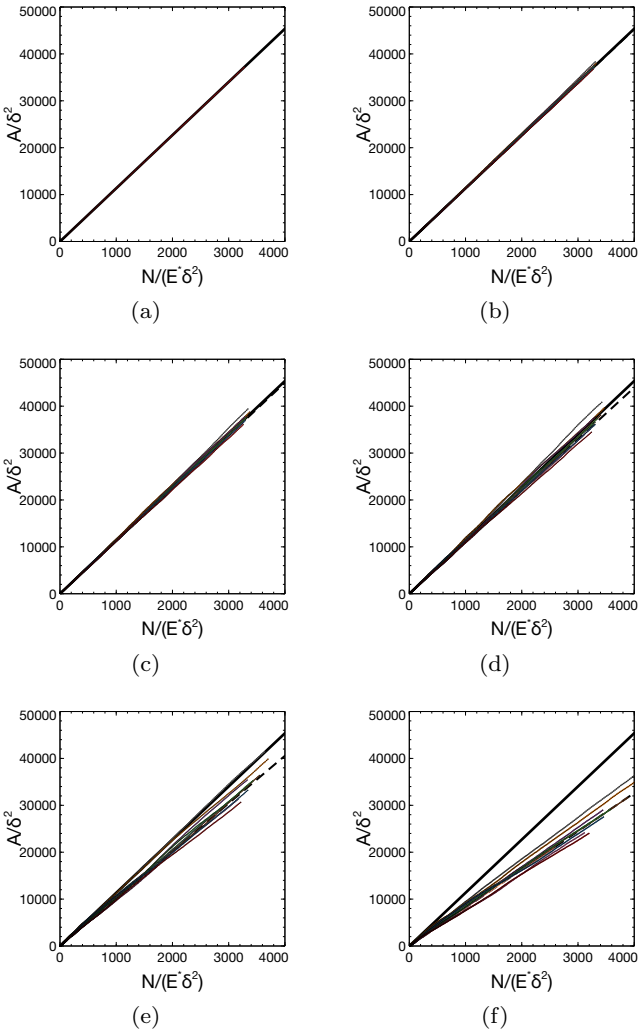

Fig. 5: Contact area vs. load curves for different values of surface roughness $h'_{\rm rms}$((a) smooth surface; (b)-(f): $h'_{\rm rms} = 0.01, 0.02, 0.04, 0.08, 0.16$, respectively). The thick solid line depicts the theoretical behaviour of a smooth surface, while the dashed line corresponds to the values calculated according to eq. (12)

roughness $h'_{\rm rms}$. In order to investigate the influence of the statistical variability of the surface topography on the numerical results, we simulated the contact of a conical punch with $\alpha = 80°$ with ten surfaces for each given $h'_{\rm rms}$. In particular, to examine the difference between the two analytical expressions for $A/A_{\rm cone}$ given by eq. (6) and eq. (12), the surfaces were generated for $h'_{\rm rms}$=0.01, 0.02, 0.04, 0.08 and 0.16, corresponding roughly to the range of ρ_c from 1 to 18, i.e., in the interval of their maximum discrepancy, as shown in Figure 2.

The main results obtained from the simulations are the histories of the load N and of the contact area A for each value of the imposed approach w. Figure 5 shows, for all the values of the roughness used in the simulations, the curves representing the non-dimensional contact area A/δ^2 as a function of the imposed approach w, for all the simulated surfaces (thin lines), together with the smooth-contact theoretical solution (thick solid line), i.e., using δ^2 as a normalizing factor:

$$\frac{A_{\rm cone}}{\delta^2} = \frac{2N}{E^*\delta^2 \cot\alpha}. \tag{16}$$

In Figure 6 we present the calculated relations between the load N and the approach w. The thick line is the graph of the theoretical response for a smooth

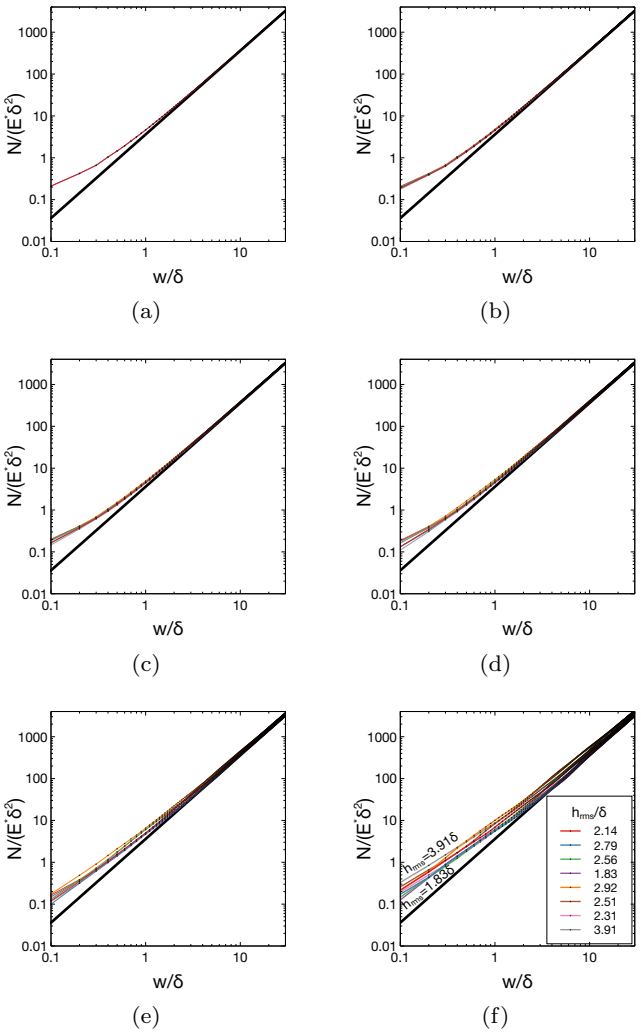

Fig. 6: Load vs. approach curves for different values of surface roughness $h'_{\rm rms}$((a) smooth surface; (b)-(f): $h'_{\rm rms} = 0.01, 0.02, 0.04, 0.08, 0.16$, respectively). The thick line depicts the theoretical curve for a smooth surface

contact, i.e., in non-dimensional form:

$$\frac{N}{E^*\delta^2} = \frac{2w^2}{\pi\delta^2 \cot\alpha}. \tag{17}$$

To evaluate the real contact area ratio $A/A_{\rm cone}$ for a given condition, both A and $A_{\rm cone}$ must be calculated at the same load N. Finding the smooth contact area $A_{\rm cone}$ as a function of load N is a trivial task: at any given approach a load N and a number of contact patches n_p are evaluated, so that $A_{\rm cone} \approx n_p\delta^2$. Icarus simulations for the case of the smooth surface agree with this result to within 0.5 % when n_p is greater than about 1000.

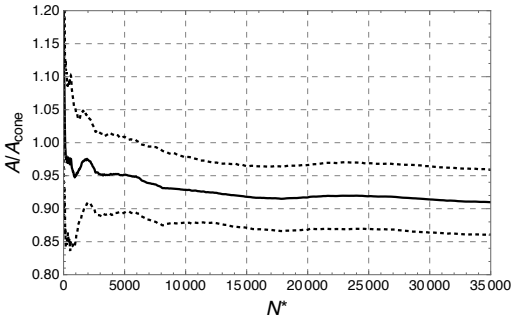

Fig. 7: Real contact area ratio $A/A_{\rm cone}$ for a 80° cone on a surface with $h'_{\rm rms} = 0.08$ vs. the normalized force N^*. Mean value (continuous line) and standard deviation (dotted lines) obtained from a sample of 10 random rough surfaces

Calculating a representative value of A for a sample of rough surfaces under a given load N is a little more involved. Since the simulations of indentation proceed by increasing the approach in discrete steps, the value of the force obtained for different surfaces under the same approach is not, in general, the same. For the surfaces of a sample with the same $h'_{\rm rms}$ the analyses were carried out determining, for each one of them, the histories of load N and number of contacts n_p up to the limit allowed by Icarus code, which depends on the size of the available computer memory. Then, a reference load, $N_{\rm ref}$, was determined as the minimum of the maximum loads. Afterwards, for each surface, the values of n_p corresponding to $N_{\rm ref}$ were calculated by interpolation, determining the mean μ_{n_p} and the standard deviation σ_{n_p} for any group of surfaces with the same $h'_{\rm rms}$. Also, the minimum value of n_p for the sample, denoted by $n_{p,{\rm ref}}$, was evaluated.

The results obtained with the procedure described above can be considered converged values, as shown in Figure 7 by the graphs of $A/A_{\rm cone}$ plotted as a function of the non-dimensional load N^* obtained dividing the calculated load by a normalizing load evaluated as the product of the theoretical mean pressure for the smooth cone $p_{m,c}$ and the area of a contact patch, δ^2:

$$N^* = \frac{2N}{\delta^2 E^* \cot\alpha}. \tag{18}$$

It can be noted that, with this position, in the case of smooth contact one has $N^* = n_p$ (i.e. the load is measured by the number of contact patches), irrespective of the cone semi-opening angle α. In Figure 7, as an example, the results for the case $h'_{\rm rms} = 0.08$ are presented, showing qualitatively the stability of the calculated mean value and standard deviation, when the number of contacts is sufficiently large.

Table 1: Influence of the roughness parameter h'_{rms} on the real contact area ratio at fixed normal load N. Comparison of Icarus output with the results of numerical integration of eq. (12). $n_{p,\mathrm{ref}}$ is the minimum number of contacting patches among the surfaces of the sample, corresponding to the load N_{ref}

h'_{rms}	$\bar{h}_{\mathrm{rms}}/\delta$	ρ_c	$n_{p,\mathrm{ref}}$	A/A_{cone} Icarus	A/A_{cone} eq. (12)	Relative error
0.00	—	—	37 164	1.000	1.000	—
0.01	0.16	17.63	37 364	1.002±0.009	0.998	0.4 %
0.02	0.32	8.82	37 470	1.001±0.017	0.992	0.9 %
0.04	0.64	4.41	37 211	0.985±0.031	0.969	1.7 %
0.08	1.29	2.20	35 152	0.909±0.045	0.894	1.7 %
0.16	2.57	1.10	30 031	0.724±0.044	0.719	0.7 %

The results in terms of number of contacts $n_{p,\mathrm{ref}}$ and area ratio A/A_{cone} are summarized in Table 1, where the output of the numerical simulations are compared with the values obtained through numerical integration of eq. (12). The graphical representation of these data is shown in Figure 2 along with the results of the theoretical model presented in sec. 2.1. The average values of the heights for each family of surfaces, $\bar{h}_{\mathrm{rms}}$, agree with the theoretical predictions of eq. (15) to within 4 %.

3 Discussion

The results obtained by means of the numerical model of the discretized contact problem, and the integration of the proposed analytical expression of the contact area ratio (eq. (12)) are in good agreement for all the possible values of the normalized pressure ρ_c, which is, according to eq. (7), a purely geometric parameter, independent of the load. Assuming the averaged outputs of the numerical simulations as reference values, the relative error of the solution obtained with our theoretical model is less than 2 % in all the investigated range of roughness, as reported in Table 1.

The influence of the introduction in the theoretical model of a variable density of contact, γ, as opposed to the constant-value assumption, can be observed in Figure 2. Consideration of the pointwise variability of the contact density gives a much better agreement than the assumption of constant density related to the mean contact pressure by eq. (6), particularly in the intermediate range of normalized mean pressure. For all the values of h'_{rms} investigated, the theoretical prediction of the contact area ratio differs less than one standard deviation from the mean value obtained with the numerical simulations.

Observation of the load vs. approach curves depicted in Figure 6 suggests that differences in roughness h_{rms} affect the response of the surfaces belonging to a family generated with the same h'_{rms}. When the approach w increases, the numerically calculated load N tends to the theoretical solution of the smooth surface, for all the values of h'_{rms}. In the initial phase of contact, when w is small, the difference between the numerical and the theoretical solution can be ascribed to the discrete nature of the contact numerical model, whose resolution is dictated by the chosen grid step δ. Furthermore, the scatter of the load vs. approach w curves increases for increasing h'_{rms}. Examination of the results obtained from all the surfaces in a family shows that there is a correlation between h_{rms} and the value of N induced by a certain w. For example, in the case of $h'_{\mathrm{rms}} = 0.16$, where $\bar{h}_{\mathrm{rms}} = 2.57\,\delta$ (Figure 6f), the lower and upper curves correspond to the minimum ($h_{\mathrm{rms}} = 1.83\,\delta$) and maximum ($h_{\mathrm{rms}} = 3.91\,\delta$), respectively. These differences in the load vs. approach response should affect the contact stiffness, but this aspect of the problem that would require a specific statistical analysis has not been pursued in this study.

4 Conclusions

In the paper, we presented the study of the contact between a conical frictionless punch and an isotropic linear-elastic halfspace bounded by a rough self-affine surface, under normal load. The focus of the analysis was on the determination of the true contact area ratio.

We assumed pressure and true contact area related by Persson's type of area - load relationship, with asymptotic saturation of the contact area for increasing pressure. In particular, these laws can be expressed by means of a constitutive parameter, i.e., a normalizing pressure depending on the equivalent elastic modulus and the rms slope, h'_{rms} of the surface. Moreover, the pressure ratio, ρ_c, given by the ratio between the cotangent of the cone angle and the rms slope is introduced as the parameter that characterizes a given cone-surface configuration.

The mean contact pressure for a smooth conical punch does not depend on the load, but only on the cone opening angle and the equivalent elastic modulus. When roughness is present, a first approximation is to consider Persson's law valid for the entire contact, using the mean pressure as a load factor, as proposed by Pastewka and Robbins for the spherical contact, obtaining the expression of eq. (6).

A more refined expression is obtained considering Persson's law to hold locally, leading to a pointwise local contact area density, (eq. (10)). Numerical integra-

tion of this function leads to an improved evaluation of the true contact area ratio.

Discrete numerical simulations show a good agreement with the predictions of the variable density theoretical model, whilst the mean pressure approximation gives poor results, overestimating the contact area ratio in the intermediate range.

The results obtained with the discrete numerical contact model show that, similarly to the smooth case, the contact area is proportional to the load, with a coefficient of proportionality decreasing for increasing surface roughness.

It has not escaped our notice that the proposed definition of a local contact area density, although applied here to a particular contact problem, suggests a possible generalization to other configurations.

Acknowledgements The authors would like to thank Professor Jim Greenwood for his kind comments on the manuscript and, in particular, for suggesting an alternative expression of the cone area ratio, shown in the Appendix.

Appendix

The expression of local contact area density, which in radially symmetrical cases has the form of eq. (10), can be derived from the procedure of integration in the pressure domain described by Manners and Greenwood [20], obtaining an expression similar to the one presented in the paper, differing only in the choice of a constitutive parameter, i.e., the normalizing pressure.

Let us introduce the following notation:

- $F_P(p) = \mathrm{Prob}(P < p)$, the cumulative distribution function of the smooth pressure distribution;
- $f_P(p) = \frac{dF_P(p)}{dp}$, the corresponding probability density function;
- $V = \frac{1}{4}E^{*2}{h'_{\mathrm{rms}}}^2$, the variance of the contact pressure needed to close all the gaps between the surfaces. This expression pertains to a 2D isotropic surface $h(x, y)$, where the orthogonal components of the slope $\partial h/\partial x$ and $\partial h/\partial y$ are uncorrelated, and similarly the pressures needed to squeeze flat the surface. While the variance of full contact pressure for a 1D profile is $V = \frac{1}{4}E^{*2}\sigma_m^2$, where $\sigma_m^2 = m_2$ is the variance of profile slopes, for a 2D surface $V = \frac{1}{4}E^{*2}\,2\sigma_m^2 = \frac{1}{2}E^{*2}\sigma_m^2 = \frac{1}{2}E^{*2}m_2 = \frac{1}{4}E^{*2}{h'_{\mathrm{rms}}}^2$, where h'_{rms} is the root mean square of the "areal roughness gradient": $h'_{\mathrm{rms}} = \sqrt{\langle|\nabla h|^2\rangle} = \sqrt{2m_2} = \sqrt{2\sigma_m^2}$.

The expression of the contact area ratio given in [20] is

$$\frac{A}{A_{\mathrm{cone}}} = \int_0^\infty f_P(p)\,\mathrm{erf}\left(\frac{p}{\sqrt{2V}}\right)\mathrm{d}p. \tag{19}$$

In radial symmetrical cases, when the radial profile of the pressure is monotone, there is a one-to-one correspondence between the pressure p and the radius r, so that a change of variable can be made, giving

$$\begin{aligned}\frac{A}{A_{\mathrm{cone}}} &= \int_a^0 f_P(p(r))\,\mathrm{erf}\left(\frac{p(r)}{\sqrt{2V}}\right)\frac{dp}{dr}\mathrm{d}r\\ &= \int_a^0 \frac{dF_P(r)}{dr}\frac{dr}{dp}\,\mathrm{erf}\left(\frac{p(r)}{\sqrt{2V}}\right)\frac{dp}{dr}\mathrm{d}r\\ &= \int_a^0 \frac{dF_P(r)}{dr}\,\mathrm{erf}\left(\frac{p(r)}{\sqrt{2V}}\right)\mathrm{d}r.\end{aligned}$$

Now, due to radial symmetry, for the conical indenter $F_P(r) = 1 - r^2/a^2$, so that $\frac{dF_P(r)}{dr} = -\frac{2r}{a^2}$. Transforming further the one-dimensional integral into a surface integral by introducing the azimuth angle ϕ, we have

$$\begin{aligned}\frac{A}{A_{\mathrm{cone}}} &= \frac{1}{\pi a^2}\int_0^{2\pi}\int_0^a r\,\mathrm{erf}\left(\frac{p(r)}{\sqrt{2V}}\right)\mathrm{d}r\mathrm{d}\phi\\ &= \frac{1}{\pi a^2}\int_0^a 2\pi r\,\mathrm{erf}\left(\frac{p(r)}{\sqrt{2V}}\right)\mathrm{d}r.\end{aligned}$$

Comparison between this expression and eq. (12) gives the local contact area density as:

$$\gamma(r) = \mathrm{erf}\left(\frac{p(r)}{\sqrt{2V}}\right).$$

Our definition of the local contact density (eq. (10)) is slightly different, due to a different choice of the normalizing pressure for the argument of the error function, i.e., $p_{\mathrm{PR}} = 2\,p_{\mathrm{rough}}/\sqrt{\pi}$ (as proposed by Pastewka and Robbins [5]), instead of $p_{\mathrm{MG}} = \sqrt{2V}$, used by Manners and Greenwood [20].

According to eq. (2), we have

$$p_{\mathrm{PR}} = \frac{2}{\sqrt{\pi}}\frac{E^* h'_{\mathrm{rms}}}{k}$$

and, by using the expression of V given above:

$$p_{\mathrm{MG}} = \frac{E^* h'_{\mathrm{rms}}}{\sqrt{2}},$$

so that, letting $k = 2$, we have $p_{\mathrm{MG}} = \sqrt{\pi/2}\,p_{\mathrm{PR}}$.

As apparent from this discussion, the definition of a local contact density leads to results coincident with those given by the integration in the pressure domain. The validity of this approach does not depend on the normalizing pressure. The choice of a certain normalizing pressure amounts to a constitutive assumption about the response of the rough interface to the value assumed by the normal pressure at a point of the contact domain.

The choice of a normalizing pressure different from the results of Persson's theory is adopted in order to get the correct linear trend, as numerically observed, in the linear range of the erf function. Since the latter covers a quite extensive region (up to contact area fraction almost of 50%), we think it is important to make this modification. However, there is more ground to this correction, since even in the case of large area fractions, there are various authors who have commented that Persson's solution may underestimate the contact area, and this comes also from a simple asperity model.

It can be shown (Greenwood, personal communication) that eq. (19) can be evaluated in quadrature as

$$\frac{A}{A_{\mathrm{cone}}} = 2\int_0^\infty \frac{\sinh q}{\cosh^3 q}\,\mathrm{erf}\left(q\frac{p_{m,c}}{\sqrt{2V}}\right)\mathrm{d}q,$$

which can be transformed, after substitution of p_{MG} with p_{PR}, into the form obtained in the paper, given by eq. (12).

References

1. Gibson RF (2014) A review of recent research on nanoindentation of polymer composites and their constituents. Compos Sci Technol 105:51 – 65
2. Love AEH (1939) Boussinesq's problem for a rigid cone. Quart J Math 10(1):161–175
3. Bhattacharya A, Nix W (1988) Finite element simulation of indentation experiments. Int J Solids Struct 24(9):881 – 891
4. Oliver WC, Pharr GM (1992) An improved technique for determining hardness and elastic modulus using load and displacement sensing indentation experiments. J Mater Res 7(6):1564–1583
5. Pastewka L, Robbins MO (2016) Contact area of rough spheres: Large scale simulations and simple scaling laws. Appl Phys Lett 108(221601):1–5
6. Persson BNJ (2002) Adhesion between an elastic body and a randomly rough hard surface. Eur Phys J E 8(4):385–401
7. Putignano C, Afferrante L, Carbone G, Demelio G (2012) The influence of the statistical properties of self-affine surfaces in elastic contacts: a numerical investigation. J Mech Phys Solids 60(5):973–982
8. Prodanov N, Dapp WB, Müser MH (2014) On the contact area and mean gap of rough, elastic contacts: dimensional analysis, numerical corrections, and reference data. Tribol Lett 53(2):433–448
9. Paggi M, Ciavarella M (2010) The coefficient of proportionality k between real contact area and load, with new asperity models. Wear 268(7–8):1020–1029
10. Yastrebov VA, Anciaux G, Molinari JF (2017) The role of the roughness spectral breadth in elastic contact of rough surfaces. J Mech Phys Solids 107:469 – 493
11. Greenwood JA, Tripp JH (1967) The elastic contact of rough spheres. J Appl Mech 34(1):153–159
12. Sneddon IN (1948) Boussinesq's problem for a rigid cone. Math Proc Camb Phil Soc 44:492–507
13. Sneddon IN (1965) The relation between load and penetration in the axisymmetric Boussinesq problem for a punch of arbitrary profile. Int J Eng Sci 3(1):47 – 57
14. Johnson KL (1985) Contact Mechanics. Cambridge University Press
15. Borri-Brunetto M, Carpinteri A, Chiaia B (1999) Scaling phenomena due to fractal contact in concrete and rock fractures. Int J Fract 95:221–238
16. Borri-Brunetto M, Chiaia B, Ciavarella M (2001) Incipient sliding of rough surfaces in contact: a multi-scale numerical analysis. Comput Methods Appl Mech Eng 190:6053–6073
17. Saupe D (1988) Algorithms for random fractals. In: Peitgen HO, Saupe D (eds) The Science of fractal images, Springer-Verlag, New York, chap 2, pp 71–113
18. Persson BNJ, Albohr O, Tartaglino U, Volokitin AI, Tosatti E (2005) On the nature of surface roughness with application to contact mechanics, sealing, rubber friction and adhesion. J Phys Condens Matter 17:R1–R62
19. Jacobs TDB, Junge T, Pastewka L (2017) Quantitative characterization of surface topography using spectral analysis. Surf Topogr: Metrol Prop 5(1):013,001
20. Manners W, Greenwood JA (2006) Some observations on Persson's diffusion theory of elastic contact. Wear 261:600–610